# Diffusivity and quantitative T1 profile of human visual white matter tracts after retinal ganglion cell damage

Hiromasa Takemura[a,b,*,1], Shumpei Ogawa[c,d,**,1], Aviv A. Mezer[e], Hiroshi Horiguchi[c], Atsushi Miyazaki[f], Kenji Matsumoto[f], Keigo Shikishima[c], Tadashi Nakano[c], Yoichiro Masuda[c]

[a] Center for Information and Neural Networks (CiNet), National Institute of Information and Communications Technology, and Osaka University, Suita, Japan
[b] Graduate School of Frontier Biosciences, Osaka University, Suita, Japan
[c] Department of Ophthalmology, The Jikei University School of Medicine, Tokyo, Japan
[d] Department of Ophthalmology, Atsugi city hospital, Atsugi, Japan
[e] The Edmond and Lily Safra Center for Brain Science, The Hebrew University of Jerusalem, Israel
[f] Brain Science Institute, Tamagawa University, Machida, Japan

## ARTICLE INFO

## ABSTRACT

In patients with retinal ganglion cell diseases, recent diffusion tensor imaging (DTI) studies have revealed structural abnormalities in visual white matter tracts such as the optic tract, and optic radiation. However, the microstructural origin of these diffusivity changes is unknown as DTI metrics involve multiple biological factors and do not correlate directly with specific microstructural properties. In contrast, recent quantitative T1 (qT1) mapping methods provide tissue property measurements relatively specific to myelin volume fractions in white matter. This study aims to improve our understanding of microstructural changes in visual white matter tracts following retinal ganglion cell damage in Leber's hereditary optic neuropathy (LHON) patients by combining DTI and qT1 measurements. We collected these measurements from seven LHON patients and twenty age-matched control subjects. For all individuals, we identified the optic tract and the optic radiation using probabilistic tractography, and evaluated diffusivity and qT1 profiles along them. Both diffusivity and qT1 measurements in the optic tract differed significantly between LHON patients and controls. In the optic radiation, these changes were observed in diffusivity but were not evident in qT1 measurements. This suggests that myelin loss may not explain trans-synaptic diffusivity changes in the optic radiation as a consequence of retinal ganglion cell disease.

## 1. Introduction

Blindness is a major sensory loss that significantly affects quality of life (Ramrattan et al., 2001) and educational opportunities (Eckert et al., 2015), and increases the risk of death (McCarty et al., 2001). Advances in modern medical treatment have enabled the prevention or cure of approximately 80% of visual impairments (Bourne et al., 2018). However, there are as yet no established therapies for hereditary retinal diseases, which affect approximately 1 in 4000 people. It is important to establish a method to measure and assess the extent of damage to the nervous system resulting from retinal diseases.

Non-invasive neuroimaging methods have advantages as a clinical tool for assessing the damage to the nervous system because they enable us to measure the structural properties of the visual system in living humans. Recently, neuroimaging studies have suggested that retinal disease may affect not only the retina, but also subsequent visual white matter tracts that support signal transmission from the retina to visual cortex. A series of diffusion tensor imaging (DTI) studies has demonstrated structural abnormalities in early visual white matter tracts, such as the optic tract or optic radiation, in amblyopia (Allen et al., 2015, 2018; Duan et al., 2015), macular degeneration (Hernowo et al., 2014; Malania et al., 2017; Prins et al., 2016a, 2016b; Yoshimine et al., 2018), and retinal ganglion cell diseases (Kaushik et al., 2014; Manners et al., 2015; Nucci et al., 2013; Ogawa et al., 2014; Wang et al., 2016; You et al., 2019; Zhou et al., 2017). Such DTI studies have improved our understanding of the relationship between neuroimaging

measurements and underlying degeneration of fiber pathways, and opened an avenue for *in vivo* assessment of disease progression along white matter tracts in individual patients.

However, the neurobiological basis of white matter changes in retinal disease revealed by DTI studies has not been well characterized, as most of studies relied on simpler DTI metrics such as Fractional Anisotropy (FA; Basser and Pierpaoli, 1996). Although FA is sensitive to various types of microstructural changes, it lacks direct correlations with specific neurobiological factors (Assaf et al., 2019; Jones et al., 2013; Rokem et al., 2017; Sampaio-Baptista and Johansen-Berg, 2017; Thomason and Thompson, 2011; Wandell and Le, 2017; Yeatman et al., 2013). It is thus challenging to interpret the abnormalities in FA within a specific neurobiological framework, such as myelin or axonal damage.

Recently, quantitative T1 (qT1) measurements have been proposed to mitigate the limitations of conventional DTI metrics (Forstmann et al., 2016; Mezer et al., 2013; Sereno et al., 2013; Weiskopf et al., 2015). This method quantifies T1 relaxation time in individual voxels by combining structural MRI measurements with multiple parameters and removing measurement biases. Converging evidence shows that qT1 provides a good approximation of myelin volume in brain tissues, consistent with histological studies (Lutti et al., 2014; Sereno et al., 2013; Stüber et al., 2014; Weiskopf et al., 2015; but see Harkins et al., 2016). Comparing DTI and qT1 approaches will improve interpretation of the microstructural properties of white matter (Berman et al., 2018; Stikov et al., 2015; Yeatman et al., 2014b).

In this study, we aimed to improve understanding of microstructural changes observed along visual white matter tracts after retinal ganglion cell damage, using a combination of DTI and qT1 measurements. To this end, we collected DTI and qT1 data from seven patients with Leber's hereditary optic neuropathy (LHON), a mitochondrial genetic disease resulting in acute or subacute bilateral damage of retinal ganglion cells and loss of central vision. Among several DTI-based metrics for white matter tissue properties, we primarily report the results on FA, which has been thoroughly tested in clinical DTI studies (Rokem et al., 2017; Thomason and Thompson, 2011). We evaluated FA and qT1 along visual white matter tracts (optic tract and optic radiation) in LHON patients, and compared FA and qT1 measurements with those in age-matched controls.

## 2. Materials and methods

We collected DTI and qT1 datasets from the LHON and control groups. We identified the trajectories of visual white matter tracts (optic tract and optic radiation) using probabilistic tractography (Sherbondy et al., 2008a, 2008b). We then evaluated tissue properties (FA and qT1) along visual tracts across both groups. The codes for reproducing figures and statistical analyses in this work are publicly available *via* the Open Science Foundation (https://osf.io/s2gmy/).

### 2.1. Subjects

Experienced ophthalmologists diagnosed LHON at the Jikei University School of Medicine, Department of Ophthalmology, Tokyo, Japan (see Table 1). All seven subjects with LHON (all males; mean age $\pm$ 1 S.D. = 28.6 $\pm$ 9.3 years; from 19 to 44 years; Table 1) were in the chronic stage and were submitted to comprehensive ophthalmological examinations, including best-corrected visual acuity, intraocular pressure, slit-lamp microscopy, fundus examination, visual field test, optical coherence tomography (OCT) and mitochondrial genetic test (see Supplementary Materials and Methods). The study size was determined by the maximum number of LHON patients under outpatient treatment at the above Department from May 2015 to December 2016, and who agreed to participate in this study. Low prevalence rate of LHON in Japan (Ueda et al., 2017) limited our recruitment to seven patients during this period. Twenty healthy volunteers (16 males and 4 females; mean age 29.7 $\pm$ 9.7 years; from

**Table 1**
LHON patients profile.

| Subject | Age | Gender | Onset | mtDNA | Idebe none | VA_R | VA_L | VF_R (vertical x horizontal) | VF_L (vertical x horizontal) | HFA_R | HFA_L | OCT (mGCL + IPL_R) | OCT (mGCL + IPL_L) |
|---|---|---|---|---|---|---|---|---|---|---|---|---|---|
| LHON1 | 35 | M | 13 | 11778 | – | 0.04 | 0.03 | V/4 30 × 15 scotoma | V/4 30 × 15 scotoma | N/A | N/A | 48 | 48 |
| LHON2 | 25 | M | 21 | 11778 | – | 0.02 | 0.02 | V/4 10 × 12 scotoma | V/4 10 × 15 scotoma | N/A | N/A | 54 | 55 |
| LHON3 | 34 | M | 29 | 11778 | – | 0.02 | 0.02 | V/4 20 × 15 scotoma | V/4 10 × 15 scotoma | –15.9 | –16.56 | 53 | 55 |
| LHON4 | 44 | M | 43 | 11778 | – | f.c. | f.c. | V/4100 × 80 scotoma | V/4100 × 80 scotoma | N/A | N/A | 48 | 48 |
| LHON5 | 20 | M | 18 | 11778 | + | 0.02 | 0.02 | N/A | N/A | –34.23 | –34.4 | 51 | 52 |
| LHON6 | 19 | M | 17 | 14484 | + | 0.8 | 0.9 | N/A | N/A | –5.27 | –5 | 66 | 64 |
| LHON7 | 23 | M | 16 | 14484 | + | 0.15 | 0.125 | N/A | N/A | –11.67 | –11.42 | 56 | 58.5 |

f.c., finger count.; VA, Visual Acuity; VF, Visual Field; HFA, Humphrey Field Analyzer.
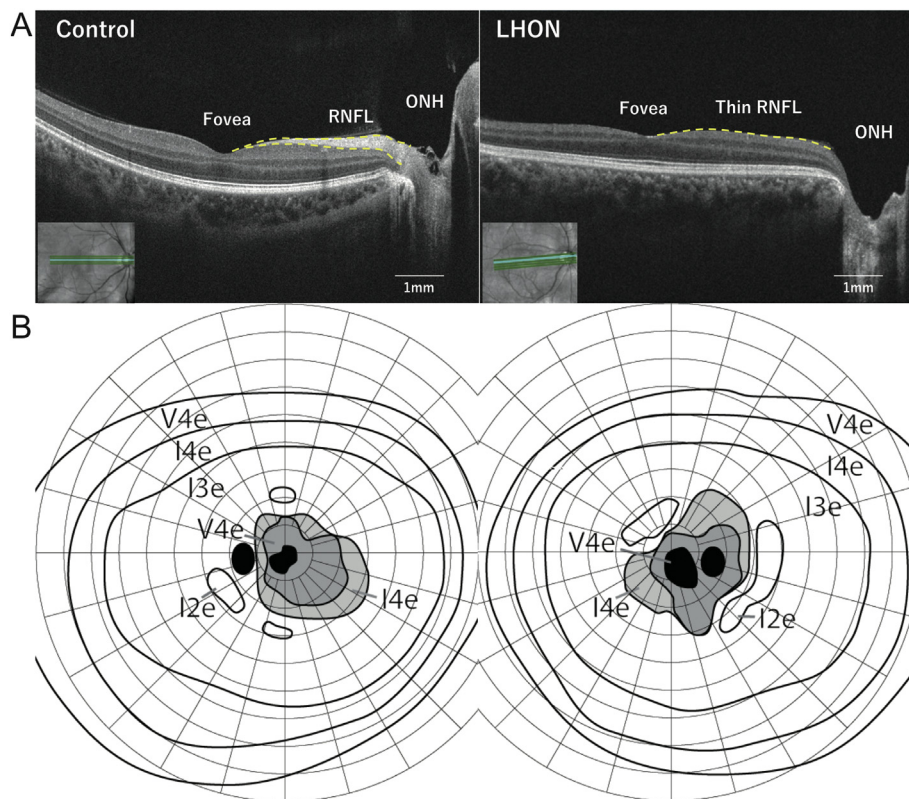
Fig. 1. A. Optical coherence tomography image of the retina in representative subjects (left panel, Healthy6; right panel, LHON3). LHON patients generally had thinner retinal nerve fiber layer thickness compared to that of healthy subjects indicating strong retinal ganglion cell damage. ONH: optic nerve head, RNFL: retinal nerve fiber layer. B. Goldmann visual field test of a representative LHON patient (LHON3) showing central visual field defect in both eyes. *Black* depicts visual field regions with no sensitivity to the target.

19 to 44 years, all with normal or corrected-to-normal vision; Supplementary Table 1) participated as controls. All subjects gave written informed consent for participation in this study, which was conducted in accordance with the ethical standards stated in the Declaration of Helsinki, and approved by the ethical committees of the Jikei University School of Medicine, and Tamagawa University.

### 2.2. Clinical features

All LHON patients had a history of sudden onset binocular central visual field loss (Fig. 1B), and were diagnosed with mitochondrial DNA (mtDNA) 14484 or 11778-point mutation (Table 1) that affect complex I subunits of the mitochondrial respiratory chain (Mackey et al., 1996). Optical coherence tomography data showed that all LHON patients showed smaller ganglion cell layer + inner pleximal layer thickness (mGCL + IPL) relative to the 1% percentile of the Asian Normative Database (Fig. 1A and Table 1; see Supplementary Information for detailed methods). Disease onset age ranged from 13 to 43 years (mean = 22.4 years old), and disease duration ranged from 1 to 22 years (mean = 6.1 years). None of the patients had a history of recovery of visual acuity. Three patients (LHON 5–7) were treated with idebenone in a clinical trial. A previous work demonstrated that vision in some patients at an early disease stage improved with a megadose (900 mg/day) of idebenone (Klopstock et al., 2011). Only one patient, LHON5, had slight right visual acuity recovery ($-0.10$ from $-0.15$). The two other patients (LHON6 and 7) had no recovery of sight after idebenone therapy.

LHON may co-occur with multiple sclerosis (Parry-Jones et al., 2008; Pfeffer et al., 2013; Vanopdenbosch et al., 2000), but none of the LHON patients in this study had any clinical history of multiple sclerosis. Furthermore, whole-brain MRI images (including T2-weighted images) collected from LHON patients were evaluated by neuroradiologists at the Jikei University School of Medicine, but no evidence of multiple sclerosis was found. Finally, T1-weighted images collected at the time of our DTI and qT1 experiments were evaluated by

two authors who are medical doctors (S.O. and H.H.), to confirm the absence of visible white matter lesions. It is therefore unlikely that the LHON patients in this study are cases of co-occurrence of LHON and multiple sclerosis.

### 2.3. MRI data acquisition

All MRI data were acquired using a 3 T SIEMENS Trio Tim scanner at Tamagawa University Brain Science Institute, Machida, Japan.

#### 2.3.1. T1-weighted structural MRI data acquisition

We collected T1-weighted MR-RAGE images (1.0 mm isotropic; repetition time [TR], 2000 ms; echo time [TE], 1.98 ms), using a 32-channel head coil, from all subjects to estimate the white/Gray matter border. The segmentation was performed using an automated procedure in Freesurfer software (https://surfer.nmr.mgh.harvard.edu/) (Fischl, 2012). The tissue segmentation was used for subsequent DTI analyses. Acquisition of the T1-weighted MRI data took approximately 9 min 17 s per subject.

#### 2.3.2. DTI data acquisition

We collected DTI data from all subjects using a 12-channel head coil. Data were acquired using single shot spin-echo echo planar imaging (EPI) sequence (TR, 7500 ms; TE, 93 ms; voxel size, $1.8 \times 1.8 \times 1.8$ mm; phase encoding direction = AP; phase partial Fourier = 6/8; 2× acceleration; diffusion scheme, monopolar). The diffusion weighting was isotropically distributed along the 12 directions (b-value = 1000 s/mm$^2$). We chose this relatively low b-value for diffusion-weighted scans in order to achieve higher signal-to-noise ratio, since the gradient strength of the SIEMENS Trio Tim system is limited (40 mT/m). In each run, diffusion-weighted measurements were repeated three times. Three non-diffusion-weighted (b = 0) images were also acquired during each run. We performed two runs of DTI scan for all subjects. Acquisition of the DTI data took approximately 10 min and 30 s per subject.

### 2.3.3. qT1 data acquisition

We measured qT1 in all subjects using a 32-channel head coil, following protocols described in previous publications (Gomez et al., 2017; Mezer et al., 2013). We measured four Fast Low Angle Shot (FLASH) images with flip angles of 4°, 10°, 20°, and 30° (TR, 12 ms; TE, 2.41 ms), and a scan resolution of 2 mm isotropic. We collected five additional spin echo inversion recovery (SEIR) scans with an echo planar imaging (EPI) readout (TR, 3000 ms; TE, 49 ms; 2× acceleration) to remove field inhomogeneities. The inversion times were 50, 200, 400, 1200, and 2400 ms. In-plane resolution and slice thickness of the additional scans were $2 \times 2 \, \text{mm}^2$ and 4 mm, respectively. Acquisition of the qT1 data took approximately 13 min and 30 s per subject.

### 2.4. MRI data analysis

### 2.4.1. DTI data preprocessing

DTI data preprocessing was performed using mrDiffusion tools implemented in the vistasoft distribution (https://github.com/vistalab/vistasoft). Diffusion-weighted images were corrected for eddy-currents, motion compensated (Rohde et al., 2004), and aligned to the structural T1-weighted images using a 14-parameter constrained nonlinear coregistration. Diffusion-weighting gradient directions were reoriented by applying the same transformation used on the diffusion-weighted images. The tensors were then fit to DTI data using a least-squares algorithm. We computed the eigenvalue decomposition of the diffusion tensor. The resulting eigenvalues were used to compute the fractional anisotropy (FA; Fig. 2B), mean diffusivity, (MD), radial diffusivity (RD), and axial diffusivity (AD) (Basser and Pierpaoli, 1996).

### 2.4.2. qT1 data preprocessing

Both the FLASH and SEIR scans were processed using the mrQ software package (https://github.com/mezera/mrQ) in MATLAB to produce the quantitative T1 (qT1; Fig. 2B) and macromolecular tissue volume (MTV) maps (Mezer et al., 2013). The mrQ analysis pipeline corrects for RF coil bias using SEIR-EPI scans, producing accurate proton density (PD) and T1 fits across the brain. We used voxels from within the ventricles to denote cerebrospinal fluid (CSF). MTV maps were produced by calculating the fraction of a voxel that was non-water (CSF voxels were classified as approximately 100% water). The full analysis pipeline and its published description can be found at https://github.com/mezera/mrQ (Mezer et al., 2013, 2016). Finally, we registered qT1 and MTV maps into T1-weighted structural MRI images using the FSL FLIRT tool to align with DTI data, which were also co-registered with identical T1-weighted images (Jenkinson et al., 2002).

### 2.4.3. Tract identification

We identified three visual white matter tracts (optic tract, optic radiation, and vertical occipital fasciculus [VOF]) from DTI data using probabilistic tractography. The optic chiasm, lateral geniculate nucleus (LGN; see Supplementary Fig. 1), and primary visual cortex (V1) were identified as regions of interest (ROIs) for tractography. The optic tract and optic radiation were identified using ConTrack (Sherbondy et al., 2008a). ConTrack initially sampled candidate streamlines between ROIs (optic tract, optic chiasm and LGN; optic radiation, LGN, and V1). The VOF streamlines were initially sampled by combining constrained spherical deconvolution-based probabilistic tractography implemented in MRtrix3 (Tournier et al., 2012) (http://www.mrtrix.org/) and open-source MATLAB code distributed with the Automated Fiber Quantification (AFQ) toolbox (Yeatman et al., 2012; https://github.com/
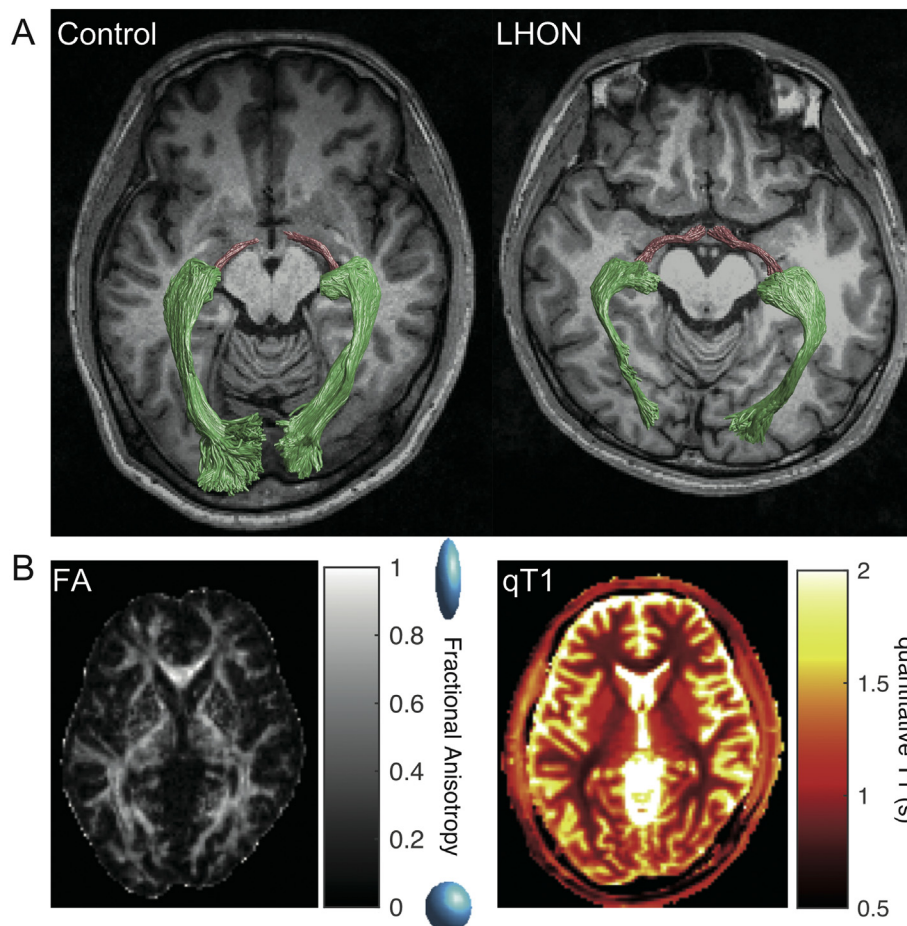


Fig. 2. A. Visual white matter tracts identified by tractography in representative subjects (left, Healthy5; right, LHON1; magenta, optic tract; green, optic radiation). Tracts are shown above an axial slice of T1-weighted image. See Supplementary Fig. 2 for examples of other subjects. B. Fractional Anisotropy (FA) and quantitative T1 (qT1) map in a representative healthy subject (Healthy5).

yeatmanlab/AFQ) following anatomical prescriptions in a previous work (Yeatman et al., 2014b). For each tract, a set of streamlines was refined by subsequent processing on outlier streamline removal. Further details on tract identification and outlier removal methods are described in the Supplementary Materials and Methods.

### 2.4.4. Evaluating tract profile

We evaluated the tissue properties of each visual white matter tract based on methods used in previous studies (Duan et al., 2015; Levin et al., 2010; Ogawa et al., 2014; Yeatman et al., 2012). Briefly, we resampled each streamline to 100 equidistant nodes. Tissue properties (FA, MD, RD, AD, qT1, and MTV) were calculated at each node of each streamline. The properties at each node were summarized by taking a weighted average of microstructural measurements (FA, MD, RD, AD, qT1, and MTV) on each streamline within that node. The weight of each streamline was based on the Mahalanobis distance from the tract core. We excluded the first and last 20 nodes from the tissue property of the tract core to exclude voxels close to gray/white matter interfaces where the tract was likely to intersect heavily with other fibers, such as the superficial U-fiber system. We summarized the profile of each tract with a vector of 60 values representing the microstructural measurements sampled at equidistant locations along the central portion of the tract. Measurements from the diffusion tensor model (FA, MD, RD, and AD) were averaged across two runs. We also demonstrated test-retest reliability of the FA analysis by dividing the analysis between two runs (Supplementary Figs. 3 and 5). Measurements from the left and right hemispheres were averaged. Inter-group differences in the major metrics of interest (FA and qT1) were assessed using the two-tailed two-sample $t$-test. We calculated the effect size (Cohen's d') of the difference between LHON and control groups for each comparison, including comparisons performed in supplementary analyses for other metrics (MD, RD, AD and MTV). We also calculated estimated volumes for the optic tract and optic radiation by counting the number of voxels intersecting with single or multiple streamlines in T1-weighted image (1 mm isotropic).

## 3. Results

We calculated two microstructural measurements (FA and qT1) derived from independent MRI scans along visual white matter tracts (optic tract and optic radiation). These tract profiles were measured in single LHON patients, and the individual patient profiles were compared with the distributions of age-matched controls to quantify structural abnormalities.

### 3.1. FA and qT1 profile along visual white matter tracts

#### 3.1.1. LHON affects both diffusivity and qT1 along the optic tract

We identified the optic tract in all 54 hemispheres (see Fig. 2A for representative subjects; see Supplementary Fig. 2 for more examples). Fig. 3 depicts a profile of FA and qT1 along the optic tract in healthy control (black) and LHON groups (blue). The gray shaded regions in Fig. 3 show the band of FA (left panel) and qT1 (right panel) control distribution along the length of the optic tract in the control group. The individual blue curves are for single LHON patients. We observed a significant group difference in both FA (Fig. 3, left; d' = 1.43; two-tailed two-sample $t$-test, $t_{25}$ = 2.83, 95% confidence interval [CI], 0.01–0.07, $P$ = 0.009) and qT1 (Fig. 3, right; d' = −1.45; two-tailed two-sample t-test, $t_{25}$ = −3.79, 95% CI, −0.18 – -0.05, $P$ = 0.0008). The effect size of FA difference was relatively small but was consistent across two independent scanning sessions (Supplementary Fig. 3; run 1, d' = 1.24; two-tailed two-sample $t$-test, $t_{25}$ = 2.49, 95% CI, 0.01–0.07, $P$ = 0.02; run 2, d' = 1.51; $t_{25}$ = 3.02, 95% CI, 0.01–0.07, $P$ = 0.006).

Since the optic tract is more susceptible to partial voluming with neighboring CSF, we performed supplementary analysis using a conservative criterion for rejecting streamlines which were distant from the streamline core (see Supplementary Material and Methods). This analysis further excludes streamlines located close to the border between CSF and the optic tract, at the expense of a reduced number of voxels, for calculation of the tract profile. As a result, the estimated the optic tract became smaller as we rejected streamlines located close to the border between CSF and the optic tract based on this criterion (Supplementary Fig. 4A). This analysis revealed a significant inter-group difference in both FA (Supplementary Fig. 4B, left; d' = 1.42; two-tailed two-sample $t$-test, $t_{25}$ = 2.81, 95% CI, 0.01–0.07, $P$ = 0.01) and qT1 (Supplementary Fig. 4B, right; d' = −1.45; two-tailed two-sample t-test, $t_{25}$ = −3.75, 95% CI, −0.18 – -0.05, $P$ = 0.0009). Since it was not possible completely to exclude partial voluming with CSF, this suggests that the observed difference in the optic tract was robust across criteria for rejecting outlier streamlines.

In sum, both FA and qT1 provided evidence of microstructural changes in the optic tract as a consequence of LHON. The increment of qT1 suggests that diffusivity changes in the optic tract may be explained by a loss of myelin or other pathological changes correlating with qT1 following retinal ganglion damage.

#### 3.1.2. LHON affects diffusivity but not qT1 along the optic radiation

We also identified the optic radiation in all 54 hemispheres (see Fig. 2A and Supplementary Fig. 2 for examples). Fig. 4 shows a profile of the FA and qT1 along the optic radiation in control (black) and LHON groups (blue). We observed a significant group difference in FA (Fig. 4, left; d' = 2.16; two-tailed two-sample $t$-test, $t_{25}$ = 4.73, 95% CI, 0.05–0.12, $P$ = 0.00008), which was reproducible across two scanning sessions (run 1, d' = 2.38; two-tailed two-sample t-test, $t_{25}$ = 5.17, 95% CI, 0.05–0.12, $P$ = 0.00002; run 2, d' = 1.95; two-tailed two-sample t-test, $t_{25}$ = 4.26, 95% CI, 0.04–0.12, $P$ = 0.0003; Supplementary Fig. 5). Inter-group differences were larger in the posterior parts of the optic radiation, consistent with a previous study (Ogawa et al., 2014).

In contrast, qT1 measurements in the LHON group were not significantly different from those in the control group (Fig. 4, right panel; d' = 0.23; two-tailed two-sample t-test, $t_{25}$ = 0.49, 95% CI, −0.03–0.04, $P$ = 0.63). A lack of significant results in qT1, a measurement that correlates with myelin volume fraction, suggests that the biological underpinnings of structural abnormalities in the optic radiation may differ from those in the optic tract.

In both FA and qT1 measurements, the degree of abnormality in optic tract and optic radiation varied among LHON patients (Figs. 3 and 4). This raises the possibility of a relationship between variability in optic tract and that in optic radiation. We found no evidence for such a correlation in either FA ($r$ = 0.10) or qT1 ($r$ = 0.07; Supplementary Fig. 6). However, lack of the evidence for a correlation may be partly explained by the fact that the small sample size of our study reduces the power to detect differences among patients.

#### 3.1.3. Diffusivity changes in optic radiation in LHON and eccentricity representation in V1

LHON primarily damages retinal ganglion cells in the foveal visual field. The optic radiation is composed of fibers terminating in different regions in V1 with different visual field coverage. We tested the degree to which diffusion abnormalities were observed specifically in the foveal subcomponent of the optic radiation. We identified optic radiation subcomponents using V1 retinotopy atlases proposed by Benson and colleagues (Benson et al., 2012, 2014). Specifically, we identified the foveal V1 (0°–3°), mid-peripheral V1 (15°–30°), and far-peripheral (30°–90°) V1 positions using Benson's atlas, and we identified the optic radiation subcomponents terminating in those V1 subregions (Yoshimine et al., 2018).

Fig. 5 depicts examples of optic radiation subcomponents with endpoints near foveal, mid-peripheral, and far-peripheral V1 as well as FA and qT1 measurements along each subcomponent. We found a large effect of group differences in FA between LHON and control groups along the foveal optic radiation (d' = 2.29; two-tailed two-sample t-
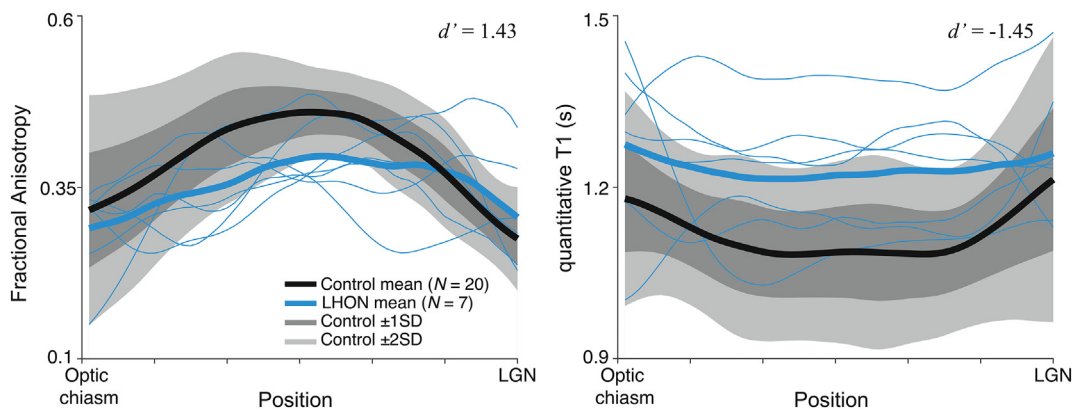
**Fig. 3.** Tissue properties along the core of the optic tract. The two panels show the FA measures (left panel) and qT1 measures (right panel) in the optic tract, respectively. Profiles of individual LHON patients are depicted as thin blue curves. Thick curves show the mean of each group (LHON: blue, healthy control: black). The lighter gray shades show a range of ± 2 S.D. from the control mean, and the darker gray band shows ± 1 S.D. from the control mean. The horizontal axis describes normalized position along the tract.

test, $t_{25}$ = 4.85, 95% CI, 0.05–0.11, $P$ = 0.00006). Group differences in mid-peripheral or far-peripheral optic radiation were significant, but effect sizes were smaller (mid-periphery: d' = 0.98; two-tailed two-sample t-test, $t_{25}$ = 2.15, 95% CI, 0.00–0.07, $P$ = 0.04; far-periphery: d' = 0.89; two-tailed two-sample t-test, $t_{25}$ = 2.22, 95% CI, 0.00–0.06, $P$ = 0.04). We did not observe a significant group difference in qT1 measurement along all three optic radiation subcomponents (fovea: d' = 0.09; two-tailed two-sample t-test, $t_{25}$ = 0.17, 95% CI, −0.04–0.04, $P$ = 0.86; mid-periphery: d' = 0.61; two-tailed two-sample t-test, $t_{25}$ = 1.33, 95% CI, −0.01–0.06, $P$ = 0.20; far-periphery: d' = 0.65; two-tailed two-sample t-test, $t_{25}$ = 1.54, 95% CI, −0.01–0.05, $P$ = 0.14). These results suggest that in LHON, abnormalities in diffusivity in the optic radiation can be most clearly identified along the subcomponent which has endpoints near foveal V1, although we do not exclude the possibilities that the small effect size for other subcomponents can be explained by the relative difficulty in fiber tracking, or differences in signal-to-noise ratio.

### 3.2. qT1 measurements are consistent with anatomy of the optic radiation

qT1 measures the longitudinal (T1) relaxation rate, with units of seconds. This rate depends on the amount and type of tissues in a voxel. A voxel that has a substantial lipid component has smaller (shorter) qT1 values compared with one filled with water. Recent studies reported that the myelin volume fraction is a particularly important factor explaining across-voxel variations of qT1 in white matter (Stüber et al., 2014). Currently, it is widely accepted that heavily myelinated regions have smaller qT1 values (Sereno et al., 2013; Stüber et al., 2014; Yeatman et al., 2014b).

In this study, we measured qT1 in a clinically feasible scan time and spatial resolution (see Materials and Methods). In order to clarify the validity of qT1 measurement in this experiment, we compared the properties of qT1 with known anatomy. The Vertical Occipital Fasciculus (VOF) is a fiber tract connecting the dorsal and ventral occipital cortices (Takemura et al., 2016; Wu et al., 2016; Yeatman et al., 2014b) and is located lateral to the optic radiation (Takemura et al., 2017). Classical anatomical studies using myelin staining have shown that the optic radiation is more myelinated than is the VOF (Schurr et al., 2018; Takemura et al., 2018; Vogt, 1904). More recently, Yeatman et al. (2014b) replicated this observation using qT1 measurements from living humans, such that the VOF could be distinguished in a qT1 map from adjacent white matter, including the optic radiation, by differences in myelin volume fractions.

We performed similar analyses to those of Yeatman et al. (2014b) to verify consistency across qT1 measurements in this study and previous histological findings (Fig. 6A). While the voxel size of the qT1 map in our study was relatively coarse (2 mm isotropic), the properties of the qT1 map in the occipital cortex were highly consistent with histological studies and findings reported in Yeatman et al. (2014b). The medial side of the white matter near the calcarine sulcus, which includes the optic radiation, has smaller qT1 values compared with lateral white matter including the VOF (Fig. 6A). This observation was consistent across subjects in both control and LHON groups. In both control and LHON groups, qT1 value in VOF was significantly larger than that in the optic radiation (Fig. 6B; control, d' = 1.53; two-tailed paired t-test, $t_{38}$ = 8.81, 95% CI, 0.05–0.07, $P$ = 0.00000004; LHON, d' = 1.91, two-tailed paired t-test, $t_{12}$ = 4.26, 95% CI, 0.02–0.09, $P$ = 0.005). These results indicate that qT1 measurement in our study successfully
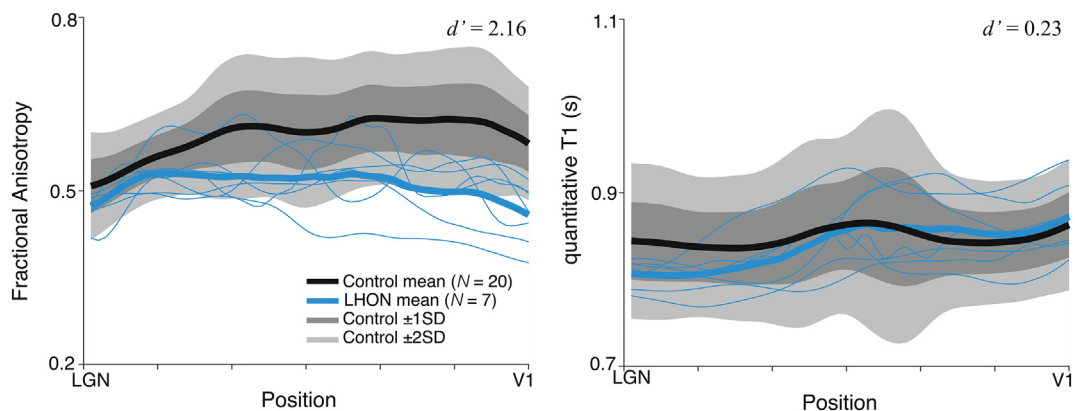


**Fig. 4.** Tissue properties along the core of the optic radiation (left, FA; right, qT1). The conventions are identical to those used in Fig. 3.
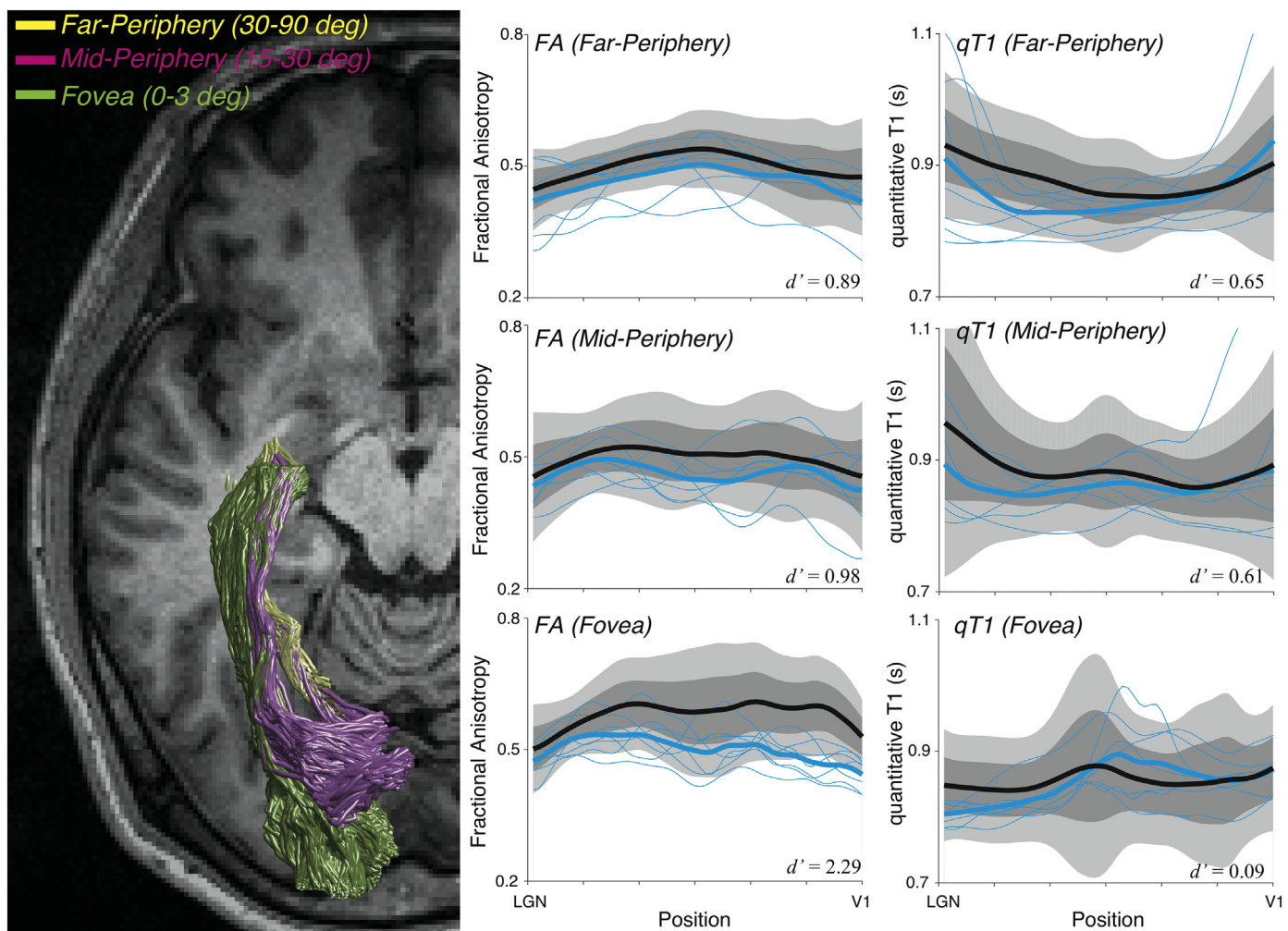
**Fig. 5.** Diffusivity and qT1 measurements along subcomponents of the optic radiation terminating near far-peripheral V1 (yellow, left figure), mid-peripheral V1 (magenta, left figure), and foveal V1 (green, left figure). The measurements of FA and qT1 for each subcomponent (upper row; far-periphery; middle row: mid-periphery; lower row: fovea) are shown in the middle (FA) and right panels (qT1). The largest group difference between LHON (cyan) and control (black) groups was found in FA measurements in foveal V1. The conventions of middle and right panels are identical to those used in Figs. 2 and 3.
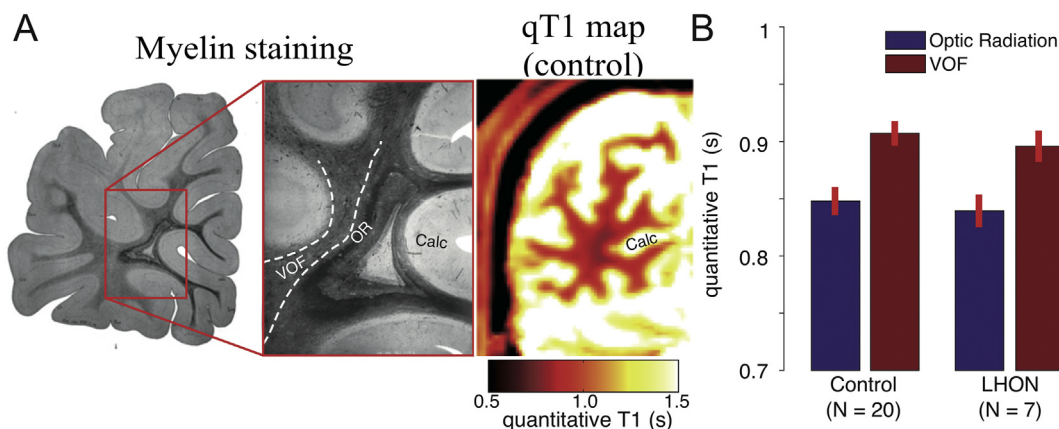


**Fig. 6.** Comparison of myelin staining and qT1 maps collected in this study. A. Classical anatomical studies and qT1 maps measured in this study. *Left:* Coronal slice of post-mortem section from Vogt (1904) stained for myelin. The vertical occipital fasciculus (VOF) stains lighter than the optic radiation (OR) because the VOF is less myelinated. Calc: Calcarine sulcus. The panel is reproduced from Yeatman et al. (2014b). *Right:* Coronal slice of qT1 map in a representative subject (Healthy5) in this study. Similar to myelin staining, the medial side of white matter near the calcarine sulcus (optic radiation) has smaller qT1 compared with that of lateral white matter (VOF). B. Comparison of qT1 across the optic radiation and VOF in the control and LHON groups. In both groups, the optic radiation has smaller qT1 compared with that of VOF, which is consistent with known anatomy. Error bar indicates ± 1 S.E.M.
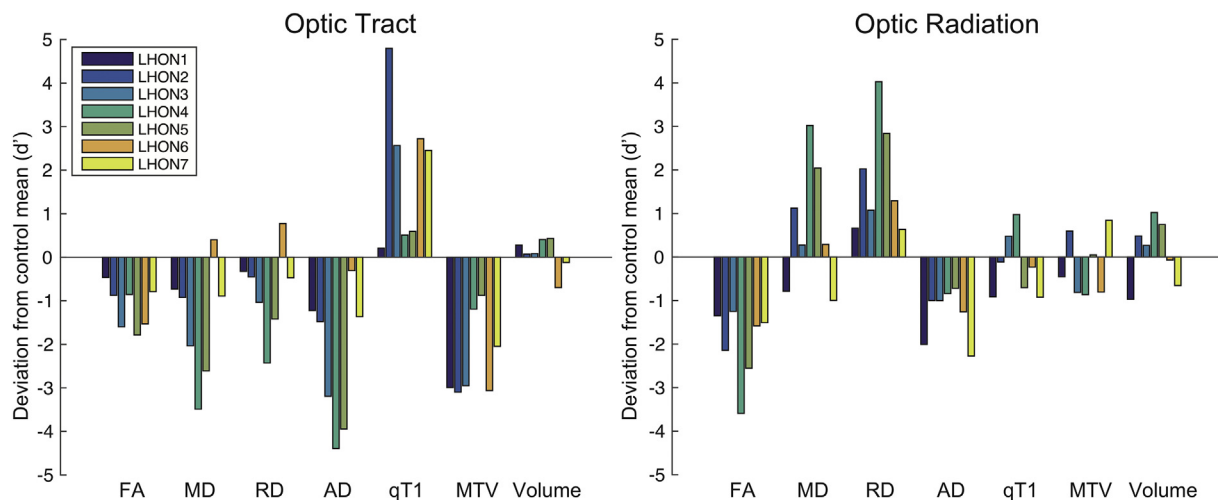
**Fig. 7.** Evaluation of different MRI metrics (diffusivity, qT1 and MTV) and tract volume. *Left panel*: optic tract. *Right panel*: optic radiation. The vertical axis of each plot represents the degree to which individual LHON patients (colored bars) deviate from the control mean. The unit of vertical axis is the effect size (*d'*) of the difference between individual LHON patients and the control mean.

distinguished heavily myelinated optic radiation from less myelinated VOF. This comparison also suggests that it is unlikely that the lack of inter-group differences in qT1 along the optic radiation that we report reflects errors in qT1 measurements, because the measurements were sensitive enough to differentiate between the optic radiation and VOF.

### 3.3. Comparison across multiple MRI-based tissue property metrics

FA values in diffusion measurements were computed from the axial diffusivity (AD) and radial diffusivity (RD). Mean diffusivity (MD) has also often been used to quantify structural abnormalities in brain tissues. In addition to qT1, Macromolecular Tissue Volume (MTV) has been proposed as a quantitative measure of white matter tissues based on proton-density mapping (Berman et al., 2018; Duval et al., 2017; Mezer et al., 2013). It may be informative to report profiles of these metrics in optic tract and optic radiation to further understand the underpinnings of results found in the major metrics of interest (FA and qT1).

Fig. 7 summarizes how each MRI metric in individual LHON patients deviated from the control mean. In this analysis, the vertical axis indicates an effect size of the difference ($d'$) between individual LHON patients and the control mean for each MRI metric. There were notable differences between the optic tract and optic radiation. In the optic tract, we observed a decrease in all diffusivity measurements (FA, MD, RD and AD; effect size of group difference, $d' = 1.43, 1.26, 0.76$ and 1.74 respectively). The effect size in the optic tract was larger in AD than in RD, consistent with a previous study (Ogawa et al., 2014). We also observed a decrease of MTV in LHON patients ($d' = 2.37$), similar to observations in qT1 ($d' = -1.49$, as shown in Fig. 3). Supplementary Fig. 7 shows the tract profile of the optic tract for MD, RD, AD and MTV.

In contrast, in the optic radiation, we observed an increase in RD ($d' = -1.58$) in LHON patients, also consistent with a previous study (Ogawa et al., 2014). Additionally, we observed a decrease in AD along the optic radiation of LHON patients ($d' = 1.57$). The large effect on FA ($d' = 2.16$; Fig. 4) in the optic radiation can be explained by both an increment in RD and a decrement in AD. In contrast, increases in MD along the optic radiation were not consistent across LHON patients (Fig. 7; $d' = -0.57$). We did not find a consistent decrease of MTV across LHON patients ($d' = 0.24$), similar to observations in qT1 ($d' = 0.23$). Supplementary Fig. 8 shows the tract profile of the optic radiation for MD, RD, AD and MTV. In sum, these differences in profiles further support the idea that the tissue changes occurring in LHON patients differ between the optic tract and the optic radiation.

Finally, we compared the estimated tract volumes of LHON patients with those of control means (Fig. 7). We did not detect any significant differences in estimated tract volume between control and LHON groups for either the optic tract or optic radiation (optic tract; $d' = -0.08$; mean estimated volume in control, 425.80 mm$^3$; mean estimated volume in LHON, 435.29 mm$^3$; optic radiation; $d' = -0.13$; mean estimated volume in control, 8347.83 mm$^3$; mean estimated volume in LHON, 8750.93 mm$^3$), suggesting that microstructural differences between LHON and control subjects may be independent of macroscopic changes in tract volume.

### 4. Discussion

We evaluated tissue changes in the optic tract and optic radiation in LHON using two independent measurement technologies, DTI and qT1. We observed a significant decrease in FA and increase in qT1 in the optic tract of LHON patients compared to those of healthy controls. However, the nature of the abnormalities in the optic radiation measured by DTI and qT1 differed from that in the optic tract. In the optic radiation, we observed a significant decrease in FA in LHON patients, but no significant difference was observed in qT1. These results suggest that among LHON patients there are differences in the type of white matter tissue abnormalities between these two tracts, and that myelin loss may not be a major biological cause of diffusivity changes in the optic radiation of LHON patients.

### 4.1. What type of microstructural changes explain diffusivity abnormality along visual white matter tracts in LHON?

This study provides evidence that the properties of white matter tissue changes in LHON differ between the optic tract and the optic radiation. A previous DTI study interpreted diffusivity changes in the optic radiation following retinal disease as anterograde trans-synaptic degeneration, which is commonly observed in neurological disorders (Ogawa et al., 2014). Other studies reported atrophy in human LGN and V1 following loss of an eye or glaucoma, suggesting the occurrence of trans-synaptic degeneration (Goldby, 1957; Gupta et al., 2006; Nucci et al., 2013; Rizzo et al., 2012). However, to our knowledge, given the lack of previous pathological work on the optic radiation in LHON, current understanding of the mechanisms underlying anterograde trans-synaptic degeneration remains limited. Our results showing a decrease in FA in the optic radiation also suggest the presence of trans-synaptic degeneration initiated by retinal ganglion cell damage, but

tissue abnormalities in trans-synaptic degeneration differed from those in fibers originating from retinal ganglion cells.

The majority of previous neuroimaging studies investigating trans-synaptic degeneration following retinal disease used conventional diffusion tensor metrics such as FA to quantify tissue abnormalities (Allen et al., 2018; Kaushik et al., 2014; Malania et al., 2017; Murai et al., 2013; Ogawa et al., 2014; Yoshimine et al., 2018). Although FA is a useful and reproducible metric with high sensitivity for white matter abnormalities (Acheson et al., 2017; Yeatman et al., 2012), FA measurements relying on simpler tensor models do not directly correlate with any specific biological factors, such as axon diameter, axon density, or myelin sheath thickness (Assaf et al., 2019; Basser and Pierpaoli, 1996; Jones et al., 2013). In contrast, qT1 is affected by types of tissues, which have different T1 relaxation times. Myelin has a particularly strong impact on qT1 measured in white matter, because myelin membranes that displace water have high cholesterol and galactocerebroside content (Coetzee et al., 1996), which have substantially shorter T1 relaxation time than that of water (Koenig et al., 1990; Kucharczyk et al., 1994). A recent study using myelin staining in white matter demonstrated a close correlation between qT1 and histological measurement of myelin (Stüber et al., 2014). Close similarity between qT1 and myelin volume fraction suggests that damage to the optic tract in LHON patients may include myelin loss or other specific pathological changes related to qT1. In contrast, a lack of significant increase of qT1 in the optic radiation suggests that myelin loss may not be a major biological cause underlying diffusivity abnormality in LHON.

If myelin loss is not a major factor, what is the major microstructural change causing diffusivity changes along the optic radiation of LHON patients? Albeit speculative, we have three possible hypotheses to explain microstructural changes in the optic radiation. The first hypothesis is that the abnormality in diffusivity may reflect axonal dysfunction. Previous DTI studies in animals revealed that diffusivity measurements were sensitive to both myelin and axon pathologies (Aung et al., 2013; Song et al., 2003). It is possible that the diffusivity changes that we observed, together with the lack of abnormalities in qT1, may reflect axonal damage. The second hypothesis is that LHON caused morphological changes in the myelin sheath that affected diffusivity, but the overall myelin volume fraction along the tract was preserved. For example, a recent study on monocular deprivation in mice reported shortened myelin internode length along the optic nerve, with preservation of myelin sheath thickness (Etxeberria et al., 2016). MRI studies evaluating the impact of such microstructural changes are lacking and such change may be mediated by axonal damage, but we speculate that shorter myelin internode length may have a limited impact on qT1 because of preserved myelin thickness. The third hypothesis is that diffusivity changes may reflect abnormalities in glia. It has been demonstrated that neurodegenerative diseases, such as glaucoma, trigger reactive gliosis and an increase in glial coverage in the optic nerve (Bosco et al., 2016; Burda and Sofroniew, 2014). We speculate that LHON may have a limited impact on myelin thickness along the optic radiation, but may trigger one or multiple microstructural changes suggested above.

### 4.2. Advantages of studying LHON as a model disease for retinal ganglion damage

We could only include a small number of patients in our study due to the low prevalence of LHON; only approximately 120 cases of newly developed LHON patients were reported in Japan during 2014 (Ueda et al., 2017). Despite this small sample size, there are several advantages for studying LHON to elucidate the microstructural changes following retinal ganglion cell damage, as compared with glaucoma. First, all LHON patients have foveal visual field loss in both eyes (Fig. 1B; Carelli, 2002; Newman and Biousse, 2004), while glaucoma has inter-patient variability in the location of visual field loss. This consistency facilitates interpretation of results from individual patients

and enables consistency across patients. By taking this advantage, we analyzed optic radiation subcomponents terminating near different parts of V1 with distinct eccentricity representation (Fig. 5). Second, compared with that for most retinal diseases, LHON is an early onset disorder (Nikoskelainen et al., 1996), permitting us to eliminate the confounding effects of aging, which significantly influences white matter properties (Lebel et al., 2012b; Yeatman et al., 2014a).

Despite our small sample size, the majority of LHON patients showed clear tissue abnormalities relative to control distributions (Figs. 3, 4 and 7). This suggests that DTI and qT1 measurements may be sensitive enough to distinguish individual patients from control distributions. We also note that diffusivity changes were consistently observed across independent scanning sessions (Supplementary Figs. 3 and 5). The sensitivity, effect size, and reproducibility of measurements in this study are encouraging for future applications of neuroimaging measurements to clinical diagnosis.

### 4.3. Related DTI studies on visual white matter tracts

Recent DTI studies provided converging evidence of tissue changes of the optic tract and optic radiation caused by other retinal diseases affecting ganglion cells, such as glaucoma (see Nuzzi et al., 2018 for a review). Several previous studies also reported white matter tissue changes in LHON similar to those that we observed (Manners et al., 2015; Milesi et al., 2012; Ogawa et al., 2014; Rizzo et al., 2012). However, ours is the first study comparing DTI (FA) and qT1 measurements to evaluate the microstructural origins of white matter tissue changes and is thus a major step toward the understanding of the biological basis of changes in diffusivity.

In addition to ganglion cell damage, previous DTI studies also reported tissue abnormality in early visual white matter tracts following photoreceptor damage, such as cone-rod dystrophy (Ogawa et al., 2014), age-related macular degeneration (Hernowo et al., 2014; Malania et al., 2017; Yoshimine et al., 2018), and retinitis pigmentosa (Ohno et al., 2015). Others demonstrated abnormalities in diffusivity along visual pathways in amblyopia patients (Allen et al., 2015, 2018; Duan et al., 2015). DTI studies on optic nerve diseases also demonstrated increases in RD and decreases in FA along the optic radiation, similar to our results (Rocca et al., 2013; Tur et al., 2016). The generalizability of findings in LHON to other retinal or optic nerve diseases is an issue that should be addressed in the future.

### 4.4. Limitations and future directions

Combining DTI and qT1 measurements, we observed that tissue changes in LHON patients differ between the optic tract and optic radiation. The precise biological mechanisms of trans-synaptic tissue changes along the optic radiation are still unclear, although myelin volume loss may not be a major factor.

There are several limitations to our study. We observed considerable inter-patient variability in the extent of FA or qT1 abnormalities (Figs. 3, 4 and 7). As discussed earlier, we only measured seven LHON patients due to the low prevalence of this disorder in Japan. While we think that a carefully chosen small sample size study focusing on a specific disease is informative, the low statistical power of our study precludes robust interpretation of how the inter-subject variabilities apparent in MRI measurements (Figs. 3 and 4) are related to heterogeneity in clinical history, such as duration from disease onset. This limits interpretations of measured differences in white matter abnormalities between the optic tract and the optic radiation, because it is difficult to disambiguate whether such differences reflect differences in the underlying neurobiological process of degeneration, or differences in the speed of disease progression to the tracts.

In this study, we used a strategy of repeated measurements of DTI for 12 angular directions. The relative advantages and disadvantages of higher angular resolution acquisition and lower angular resolution with

repeated measurement for quantifying FA have been debated (Jones, 2004; Lebel et al., 2012a). Acquisition with higher angular resolution may be advantageous to solve crossing fibers at Meyer's loop regions (Chamberland et al., 2017). Improved diffusion MRI acquisition in future studies may help tractography algorithms to more accurately identify Meyer's loop regions in the optic radiation (Chamberland et al., 2018) or improve an accuracy to segment optic radiation sub-components with respect to eccentricity representations in V1. Although greater accuracy for identifying Meyer's loop will likely be achieved with advanced acquisition in future studies, we consider our finding of a clear contrast between diffusivity and qT1 measurements in the posterior, straight portion of the optic radiation (Fig. 4) supports the main conclusion of this paper.

A previous study demonstrated that qT1 serves as a good approximation for myelin volume fraction in white matter (Stüber et al., 2014). We indeed found that our qT1 measurement along the optic radiation is consistent with observations from myelin staining (Fig. 6), suggesting that our qT1 measurements are sensitive enough to classify tissue differences between the optic radiation, and neighboring pathways that differ in the extent of myelination. However, the demonstration by Harkins et al. (2016) that qT1 in the spinal cord is correlated with axon diameter rather than myelin content, poses a challenge for generalization of qT1-myelin correlates across different brain areas. Although a correlation between qT1 and myelin volume is widely reported (Lutti et al., 2014; Sereno et al., 2013; Stüber et al., 2014), further investigations are required to establish a more definitive microstructural interpretation. One potential approach would be to combine multiple quantitative MRI techniques, such as myelin water imaging (Alonso-Ortiz et al., 2015; Deoni et al., 2008; MacKay et al., 1994) or magnetization transfer imaging (Sled et al., 2004; Yarnykh and Yuan, 2004), which may provide further information to interpret white matter microstructure.

There are ongoing efforts to establish more sophisticated biophysical models from multi-shell diffusion MRI measurements (Assaf et al., 2008; Assaf and Basser, 2005; Zhang et al., 2012), and to combine diffusion and other quantitative MRI measurements to estimate the g-ratio (Berman et al., 2018, 2019; Duval et al., 2017; Mohammadi et al., 2015; Stikov et al., 2015). Despite ambiguities in complex models prevalent in the field (Jelescu et al., 2016), improved MRI acquisition and better understanding of the relationship between MRI and anatomical measurements are facilitating growth of this active field. In future, we hope that incorporating advanced MRI measurement methods may provide opportunities to examine more specific neurobiological substrates of microstructural changes in white matter following retinal ganglion cell damage.

## 5. Conclusions

Using DTI and qT1, we observed that retinal ganglion cell damage caused substantial changes in visual white matter tracts. In the optic radiation, these changes were observed specifically using diffusivity measurements, but not evident with qT1. These results suggested that the microstructural origins of the diffusivity changes differed between the tracts. Recent studies have also suggested that qT1 values in white matter correlate with histological measurements of myelin volume fractions. Our results suggest that in patients with LHON, myelin loss partly explains the diffusivity changes in the optic tract, but not the trans-synaptic diffusivity changes in the optic radiation in patients with LHON.

## Acknowledgments

## Competing interests

Authors declare no competing interests.

## Declaration of interest

None.

## Appendix A. Supplementary data

Supplementary data to this article can be found online at https://doi.org/10.1016/j.nicl.2019.101826.

## References

Acheson, A., Wijtenburg, S.A., Rowland, L.M., Winkler, A., Mathias, C.W., Hong, L.E., Jahanshad, N., Patel, B., Thompson, P.M., McGuire, S.A., Sherman, P.M., Kochunov, P., Dougherty, D.M., 2017. Reproducibility of tract-based white matter microstructural measures using the ENIGMA-DTI protocol. Brain Behav. 7, e00615.

Allen, B., Spiegel, D.P., Thompson, B., Pestilli, F., Rokers, B., 2015. Altered white matter in early visual pathways of humans with amblyopia. Vis. Res. 114, 48–55.

Allen, B., Schmitt, M.A., Kushner, B.J., Rokers, B., 2018. Retinothalamic white matter abnormalities in amblyopia. Invest. Ophthalmol. Vis. Sci. 59, 921–929.

Alonso-Ortiz, E., Levesque, I.R., Pike, G.B., 2015. MRI-based myelin water imaging: A technical review. Magn. Reson. Med. 73, 70–81.

Assaf, Y., Basser, P.J., 2005. Composite hindered and restricted model of diffusion (CHARMED) MR imaging of the human brain. Neuroimage 27, 48–58.

Assaf, Y., Blumenfeld-Katzir, T., Yovel, Y., Basser, P.J., 2008. AxCaliber: a method for measuring axon diameter distribution from diffusion MRI. Magn. Reson. Med. 59, 1347–1354.

Assaf, Y., Johansen-Berg, H., Thiebaut de Schotten, M., 2019. The role of diffusion MRI in neuroscience. NMR Biomed. 32, e3762.

Aung, W.Y., Mar, S., Benzinger, T.L., 2013. Diffusion tensor MRI as a biomarker in axonal and myelin damage. Imaging Med. 5, 427–440.

Basser, P.J., Pierpaoli, C., 1996. Microstructural and physiological features of tissues elucidated by quantitative-diffusion-tensor MRI. J. Magn. Reson. B 111, 209–219.

Benson, N.C., Butt, O.H., Datta, R., Radoeva, P.D., Brainard, D.H., Aguirre, G.K., 2012. The retinotopic organization of striate cortex is well predicted by surface topology. Curr. Biol. 22, 2081–2085.

Benson, N.C., Butt, O.H., Brainard, D.H., Aguirre, G.K., 2014. Correction of distortion in flattened representations of the cortical surface allows prediction of V1-V3 functional organization from anatomy. PLoS Comput. Biol. 10, e1003538.

Berman, S., West, K.L., Does, M.D., Yeatman, J.D., Mezer, A.A., 2018. Evaluating g-ratio weighted changes in the corpus callosum as a function of age and sex. Neuroimage 182, 304–313.

Berman, S., Filo, S., Mezer, A.A., 2019. Modeling conduction delays in the corpus callosum using MR-measured g-ratio. Neuroimage 195, 128–139.

Bosco, A., Breen, K.T., Anderson, S.R., Steele, M.R., Calkins, D.J., Vetter, M.L., 2016. Glial coverage in the optic nerve expands in proportion to optic axon loss in chronic mouse glaucoma. Exp. Eye Res. 150, 34–43.

Bourne, R.R.A., Jonas, J.B., Bron, A.M., Cicinelli, M.V., Das, A., Flaxman, S.R., Friedman, D.S., Keeffe, J.E., Kempen, J.H., Leasher, J., Limburg, H., Naidoo, K., Pesudovs, K., Peto, T., Saadine, J., Silvester, A.J., Tahhan, N., Taylor, H.R., Varma, R., Wong, T.Y., Resnikoff, S., Vision loss expert group of the global burden of disease study, 2018. Prevalence and causes of vision loss in high-income countries and in Eastern and Central Europe in 2015: magnitude, temporal trends and projections. Br. J. Ophthalmol. 102, 575–585.

Burda, J.E., Sofroniew, M.V., 2014. Reactive gliosis and the multicellular response to CNS damage and disease. Neuron 81, 229–248.

Carelli, V., 2002. Leber's hereditary optic neuropathy. In: Schapira, A.H.V., Di Mauro, S. (Eds.), Mitochondrial Disorders in Neurology. Blue Books of Practical Neurology. Butterworth-Heinemann, Boston, pp. 115–142.

Chamberland, M., Scherrer, B., Prabhu, S.P., Madsen, J., Fortin, D., Whittingstall, K., Descoteaux, M., Warfield, S.K., 2017. Active delineation of Meyer's loop using oriented priors through MAGNEtic tractography (MAGNET). Hum. Brain Mapp. 38, 509–527.

Chamberland, M., Tax, C.M.W., Jones, D.K., 2018. Meyer's loop tractography for image-guided surgery depends on imaging protocol and hardware. Neuroimage Clin 20, 458–465.

Coetzee, T., Fujita, N., Dupree, J., Shi, R., Blight, A., Suzuki, K., Suzuki, K., Popko, B., 1996. Myelination in the absence of galactocerebroside and sulfatide: normal

structure with abnormal function and regional instability. Cell 86, 209–219.

Deoni, S.C.L., Rutt, B.K., Arun, T., Pierpaoli, C., Jones, D.K., 2008. Gleaning multi-component T1 and T2 information from steady-state imaging data. Magn. Reson. Med. 60, 1372–1387.

Duan, Y., Norcia, A.M., Yeatman, J.D., Mezer, A., 2015. The structural properties of major white matter tracts in strabismic amblyopia. Invest. Ophthalmol. Vis. Sci. 56, 5152–5160.

Duval, T., Le Vy, S., Stikov, N., Campbell, J., Mezer, A., Witzel, T., Keil, B., Smith, V., Wald, L.L., Klawiter, E., Cohen-Adad, J., 2017. g-Ratio weighted imaging of the human spinal cord in vivo. Neuroimage 145, 11–23.

Eckert, K.A., Carter, M.J., Lansingh, V.C., Wilson, D.A., Furtado, J.M., Frick, K.D., Resnikoff, S., 2015. A simple method for estimating the economic cost of productivity loss due to blindness and moderate to severe visual impairment. Ophthalmic Epidemiol. 22, 349–355.

Etxeberria, A., Hokanson, K.C., Dao, D.Q., Mayoral, S.R., Mei, F., Redmond, S.A., Ullian, E.M., Chan, J.R., 2016. Dynamic modulation of myelination in response to visual stimuli alters optic nerve conduction velocity. J. Neurosci. 36, 6937–6948.

Fischl, B., 2012. FreeSurfer. Neuroimage 62, 774–781.

Forstmann, B.U., de Hollander, G., van Maanen, L., Alkemade, A., Keuken, M.C., 2016. Towards a mechanistic understanding of the human subcortex. Nat. Rev. Neurosci. 18, 57.

Goldby, F., 1957. A note on transneuronal atrophy in the human lateral geniculate body. J. Neurol. Neurosurg. Psychiatry 20, 202–207.

Gomez, J., Barnett, M.A., Natu, V., Mezer, A., Palomero-Gallagher, N., Weiner, K.S., Amunts, K., Zilles, K., Grill-Spector, K., 2017. Microstructural proliferation in human cortex is coupled with the development of face processing. Science 355, 68–71.

Gupta, N., Ang, L.-C., Noël de Tilly, L., Bidaisee, L., Yücel, Y.H., 2006. Human glaucoma and neural degeneration in intracranial optic nerve, lateral geniculate nucleus, and visual cortex. Br. J. Ophthalmol. 90, 674–678.

Harkins, K.D., Xu, J., Dula, A.N., Li, K., Valentine, W.M., Gochberg, D.F., Gore, J.C., Does, M.D., 2016. The microstructural correlates of T1 in white matter. Magn. Reson. Med. 75, 1341–1345.

Hernowo, A.T., Prins, D., Baseler, H.A., Plank, T., Gouws, A.D., Hooymans, J.M.M., Morland, A.B., Greenlee, M.W., Cornelissen, F.W., 2014. Morphometric analyses of the visual pathways in macular degeneration. Cortex 56, 99–110.

Jelescu, I.O., Veraart, J., Fieremans, E., Novikov, D.S., 2016. Degeneracy in model parameter estimation for multi-compartmental diffusion in neuronal tissue. NMR Biomed. 29, 33–47.

Jenkinson, M., Bannister, P., Brady, M., Smith, S., 2002. Improved optimization for the robust and accurate linear registration and motion correction of brain images. Neuroimage 17, 825–841.

Jones, D.K., 2004. The effect of gradient sampling schemes on measures derived from diffusion tensor MRI: a Monte Carlo study. Magn. Reson. Med. 51, 807–815.

Jones, D.K., Knosche, T.R., Turner, R., 2013. White matter integrity, fiber count, and other fallacies: the do's and don'ts of diffusion MRI. Neuroimage 73, 239–254.

Kaushik, M., Graham, S.L., Wang, C., Klistorner, A., 2014. A topographical relationship between visual field defects and optic radiation changes in glaucoma. Invest. Ophthalmol. Vis. Sci. 55, 5770–5775.

Klopstock, T., Yu-Wai-Man, P., Dimitriadis, K., Rouleau, J., Heck, S., Bailie, M., Atawan, A., Chattopadhyay, S., Schubert, M., Garip, A., Kernt, M., Petraki, D., Rummey, C., Leinonen, M., Metz, G., Griffiths, P.G., Meier, T., Chinnery, P.F., 2011. A randomized placebo-controlled trial of idebenone in Leber's hereditary optic neuropathy. Brain 134, 2677–2686.

Koenig, S.H., Brown, R.D., Spiller, M., Lundbom, N., 1990. Relaxometry of brain: why white matter appears bright in MRI. Magn. Reson. Med. 14, 482–495.

Kucharczyk, W., Macdonald, P.M., Stanisz, G.J., Henkelman, R.M., 1994. Relaxivity and magnetization transfer of white matter lipids at MR imaging: importance of cere-brosides and pH. Radiology 192, 521–529.

Lebel, C., Benner, T., Beaulieu, C., 2012a. Six is enough? Comparison of diffusion para-meters measured using six or more diffusion-encoding gradient directions with de-terministic tractography. Magn. Reson. Med. 68, 474–483.

Lebel, C., Gee, M., Camicioli, R., Wieler, M., Martin, W., Beaulieu, C., 2012b. Diffusion tensor imaging of white matter tract evolution over the lifespan. Neuroimage 60, 340–352.

Levin, N., Dumoulin, S.O., Winawer, J., Dougherty, R.F., Wandell, B.A., 2010. Cortical maps and white matter tracts following long period of visual deprivation and retinal image restoration. Neuron 65, 21–31.

Lutti, A., Dick, F., Sereno, M.I., Weiskopf, N., 2014. Using high-resolution quantitative mapping of R1 as an index of cortical myelination. Neuroimage 93 (Pt 2), 176–188.

MacKay, A., Whittall, K., Adler, J., Li, D., Paty, D., Graeb, D., 1994. In vivo visualization of myelin water in brain by magnetic resonance. Magn. Reson. Med. 31, 673–677.

Mackey, D.A., Oostra, R.J., Rosenberg, T., Nikoskelainen, E., Bronte-Stewart, J., Poulton, J., Harding, A.E., Govan, G., Bolhuis, P.A., Norby, S., 1996. Primary pathogenic mtDNA mutations in multigeneration pedigrees with Leber hereditary optic neuro-pathy. Am. J. Hum. Genet. 59, 481–485.

Malania, M., Konrad, J., Jägle, H., Werner, J.S., Greenlee, M.W., 2017. Compromised integrity of central visual pathways in patients with macular degeneration. Invest. Ophthalmol. Vis. Sci. 58, 2939–2947.

Manners, D.N., Rizzo, G., La Morgia, C., Tonon, C., Testa, C., Barboni, P., Malucelli, E., Valentino, M.L., Caporali, L., Strobbe, D., Carelli, V., Lodi, R., 2015. Diffusion tensor imaging mapping of brain white matter pathology in mitochondrial optic neuro-pathies. AJNR. Am. J. Neuroradiol. 36, 1259–1265.

McCarty, C.A., Nanjan, M.B., Taylor, H.R., 2001. Vision impairment predicts 5 year mortality. Br. J. Ophthalmol. 85, 322–326.

Mezer, A., Yeatman, J.D., Stikov, N., Kay, K.N., Cho, N.J., Dougherty, R.F., Perry, M.L., Parvizi, J., Hua le, H., Butts-Pauly, K., Wandell, B.A., 2013. Quantifying the local

tissue volume and composition in individual brains with magnetic resonance ima-ging. Nat. Med. 19, 1667–1672.

Mezer, A., Rokem, A., Berman, S., Hastie, T., Wandell, B.A., 2016. Evaluating quantitative proton-density-mapping methods. Hum. Brain Mapp. 37, 3623–3635.

Milesi, J., Rocca, M.A., Bianchi-Marzoli, S., Petrolini, M., Pagani, E., Falini, A., Comi, G., Filippi, M., 2012. Patterns of white matter diffusivity abnormalities in Leber's her-editary optic neuropathy: a tract-based spatial statistics study. J. Neurol. 259, 1801–1807.

Mohammadi, S., Carey, D., Dick, F., Diedrichsen, J., Sereno, M.I., Reisert, M., Callaghan, M.F., Weiskopf, N., 2015. Whole-brain in-vivo measurements of the axonal g-ratio in a group of 37 healthy volunteers. Front. Neurosci. 9, 441.

Murai, H., Suzuki, Y., Kiyosawa, M., Tokumaru, A.M., Ishii, K., Mochizuki, M., 2013. Positive correlation between the degree of visual field defect and optic radiation damage in glaucoma patients. Jpn. J. Ophthalmol. 57, 257–262.

Newman, N.J., Biousse, V., 2004. Hereditary optic neuropathies. Eye 18, 1144–1160.

Nikoskelainen, E.K., Huoponen, K., Juvonen, V., Lamminen, T., Nummelin, K., Savontaus, M.L., 1996. Ophthalmologic findings in Leber hereditary optic neuropathy, with special reference to mtDNA mutations. Ophthalmology 103, 504–514.

Nucci, C., Martucci, A., Cesareo, M., Mancino, R., Russo, R., Bagetta, G., Cerulli, L., Garaci, F.G., 2013. Brain involvement in glaucoma: advanced neuroimaging for un-derstanding and monitoring a new target for therapy. Curr. Opin. Pharmacol. 13, 128–133.

Nuzzi, R., Dallorto, L., Rolle, T., 2018. Changes of visual pathway and brain connectivity in glaucoma: a systematic review. Front. Neurosci. 12, 363.

Ogawa, S., Takemura, H., Horiguchi, H., Terao, M., Haji, T., Pestilli, F., Yeatman, J.D., Tsuneoka, H., Wandell, B.A., Masuda, Y., 2014. White matter consequences of retinal receptor and ganglion cell damage. Invest. Ophthalmol. Vis. Sci. 55, 6976–6986.

Ohno, N., Murai, H., Suzuki, Y., Kiyosawa, M., Tokumaru, A.M., Ishii, K., Ohno-Matsui, K., 2015. Alteration of the optic radiations using diffusion-tensor MRI in patients with retinitis pigmentosa. Br. J. Ophthalmol. 99, 1051–1054.

Parry-Jones, A.R., Mitchell, J.D., Gunarwardena, W.J., Shaunak, S., 2008. Leber's her-editary optic neuropathy associated with multiple sclerosis: Harding's syndrome. Pract. Neurol. 8, 118–121.

Pfeffer, G., Burke, A., Yu-Wai-Man, P., Compston, D.A.S., Chinnery, P.F., 2013. Clinical features of MS associated with Leber hereditary optic neuropathy mtDNA mutations. Neurology 81, 2073–2081.

Prins, D., Hanekamp, S., Cornelissen, F.W., 2016a. Structural brain MRI studies in eye diseases: are they clinically relevant? A review of current findings. Acta Ophthalmol. 94, 113–121.

Prins, D., Plank, T., Baseler, H.A., Gouws, A.D., Beer, A., Morland, A.B., Greenlee, M.W., Cornelissen, F.W., 2016b. Surface-based analyses of anatomical properties of the visual cortex in macular degeneration. PLoS ONE 11, e0146684.

Ramrattan, R.S., Wolfs, R.C., Panda-Jonas, S., Jonas, J.B., Bakker, D., Pols, H.A., Hofman, A., de Jong, P.T., 2001. Prevalence and causes of visual field loss in the elderly and associations with impairment in daily functioning: the Rotterdam Study. Arch. Ophthalmol. 119, 1788–1794.

Rizzo, G., Tozer, K.R., Tonon, C., Manners, D., Testa, C., Malucelli, E., Valentino, M.L., La Morgia, C., Barboni, P., Randhawa, R.S., Ross-Cisneros, F.N., Sadun, A.A., Carelli, V., Lodi, R., 2012. Secondary post-geniculate involvement in Leber's hereditary optic neuropathy. PLoS ONE 7, e50230.

Rocca, M.A., Mesaros, S., Preziosa, P., Pagani, E., Stosic-Opincal, T., Dujmovic-Basuroski, I., Drulovic, J., Filippi, M., 2013. Wallerian and trans-synaptic degeneration con-tribute to optic radiation damage in multiple sclerosis: a diffusion tensor MRI study. Mult. Scler. 19, 1610–1617.

Rohde, G.K., Barnett, A.S., Basser, P.J., Marenco, S., Pierpaoli, C., 2004. Comprehensive approach for correction of motion and distortion in diffusion-weighted MRI. Magn. Reson. Med. 51, 103–114.

Rokem, A., Takemura, H., Bock, A.S., Scherf, K.S., Behrmann, M., Wandell, B.A., Fine, I., Bridge, H., Pestilli, F., 2017. The visual white matter: The application of diffusion MRI and fiber tractography to vision science. J. Vis. 17, 4.

Sampaio-Baptista, C., Johansen-Berg, H., 2017. White matter plasticity in the adult brain. Neuron 96, 1239–1251.

Schurr, R., Duan, Y., Norcia, A.M., Ogawa, S., Yeatman, J.D., Mezer, A.A., 2018. Tractography optimization using quantitative T1 mapping in the human optic ra-diation. Neuroimage 181, 645–658.

Sereno, M.I., Lutti, A., Weiskopf, N., Dick, F., 2013. Mapping the human cortical surface by combining quantitative T(1) with retinotopy. Cereb. Cortex 23, 2261–2268.

Sherbondy, A.J., Dougherty, R.F., Ben-Shachar, M., Napel, S., Wandell, B.A., 2008a. ConTrack: finding the most likely pathways between brain regions using diffusion tractography. J. Vis. 8, 15.1–16.

Sherbondy, A.J., Dougherty, R.F., Napel, S., Wandell, B.A., 2008b. Identifying the human optic radiation using diffusion imaging and fiber tractography. J. Vis. 8, 12.1–11.

Sled, J.G., Levesque, I., Santos, A.C., Francis, S.J., Narayanan, S., Brass, S.D., Arnold, D.L., Pike, G.B., 2004. Regional variations in normal brain shown by quantitative mag-netization transfer imaging. Magn. Reson. Med. 51, 299–303.

Song, S.-K., Sun, S.-W., Ju, W.-K., Lin, S.-J., Cross, A.H., Neufeld, A.H., 2003. Diffusion tensor imaging detects and differentiates axon and myelin degeneration in mouse optic nerve after retinal ischemia. Neuroimage 20, 1714–1722.

Stikov, N., Campbell, J.S.W., Stroh, T., Lavelée, M., Frey, S., Novek, J., Nuara, S., Ho, M.-K., Bedell, B.J., Dougherty, R.F., Leppert, I.R., Boudreau, M., Narayanan, S., Duval, T., Cohen-Adad, J., Picard, P.-A., Gasecka, A., Côté, D., Pike, G.B., 2015. In vivo histology of the myelin g-ratio with magnetic resonance imaging. Neuroimage 118, 397–405.

Stüber, C., Morawski, M., Schafer, A., Labadie, C., Wahnert, M., Leuze, C., Streicher, M., Barapatre, N., Reimann, K., Geyer, S., Spemann, D., Turner, R., 2014. Myelin and iron concentration in the human brain: a quantitative study of MRI contrast. Neuroimage

93 (Pt 1), 95–106.

Takemura, H., Rokem, A., Winawer, J., Yeatman, J.D., Wandell, B.A., Pestilli, F., 2016. A major human white-matter pathway between dorsal and ventral visual cortex. Cereb. Cortex 26, 2205–2214.

Takemura, H., Pestilli, F., Weiner, K.S., Keliris, G.A., Landi, S.M., Sliwa, J., Ye, F.Q., Barnett, M.A., Leopold, D.A., Freiwald, W.A., Logothetis, N.K., Wandell, B.A., 2017. Occipital white matter tracts in human and macaque. Cereb. Cortex 27, 3346–3359.

Takemura, H., Pestilli, F., Weiner, K.S., 2018. Comparative neuroanatomy: integrating classic and modern methods to understand association fibers connecting dorsal and ventral visual cortex. Neurosci. Res. https://doi.org/10.1016/j.neures.2018.10.011.

Thomason, M.E., Thompson, P.M., 2011. Diffusion imaging, white matter, and psychopathology. Annu. Rev. Clin. Psychol. 7, 63–85.

Tournier, J.D., Calamante, F., Connelly, A., 2012. MRtrix: Diffusion tractography in crossing fiber regions. Int. J. Imaging Syst. Technol. 22, 53–66.

Tur, C., Goodkin, O., Altmann, D.R., Jenkins, T.M., Miszkiel, K., Mirigliani, A., Fini, C., Gandini Wheeler-Kingshott, C.A.M., Thompson, A.J., Ciccarelli, O., Toosy, A.T., 2016. Longitudinal evidence for anterograde trans-synaptic degeneration after optic neuritis. Brain 139, 816–828.

Ueda, K., Morizane, Y., Shiraga, F., Shikishima, K., Ishikawa, H., Wakakura, M., Nakamura, M., 2017. Nationwide epidemiological survey of Leber hereditary optic neuropathy in Japan. J. Epidemiol. 27, 447–450.

Vanopdenbosch, L., Dubois, B., D'Hooghe, M.B., Meire, F., Carton, H., 2000. Mitochondrial mutations of Leber's hereditary optic neuropathy: a risk factor for multiple sclerosis. J. Neurol. 247, 535–543.

Vogt, O., 1904. Neurobiologische Arbeiten. Fischer.

Wandell, B.A., Le, R.K., 2017. Diagnosing the Neural Circuitry of Reading. Neuron 96, 298–311.

Wang, J., Li, T., Sabel, B.A., Chen, Z., Wen, H., Li, J., Xie, X., Yang, D., Chen, W., Wang, N., Xian, J., He, H., 2016. Structural brain alterations in primary open angle glaucoma: a 3T MRI study. Sci. Rep. 6, 18969.

Weiskopf, N., Mohammadi, S., Lutti, A., Callaghan, M.F., 2015. Advances in MRI-based computational neuroanatomy: from morphometry to in-vivo histology. Curr. Opin.

Neurol. 28, 313–322.

Wu, Y., Sun, D., Wang, Y., Wang, Y., Wang, Y., 2016. Tracing short connections of the temporo-parieto-occipital region in the human brain using diffusion spectrum imaging and fiber dissection. Brain Res. 1646, 152–159.

Yarnykh, V.L., Yuan, C., 2004. Cross-relaxation imaging reveals detailed anatomy of white matter fiber tracts in the human brain. Neuroimage 23, 409–424.

Yeatman, J.D., Dougherty, R.F., Myall, N.J., Wandell, B.A., Feldman, H.M., 2012. Tract profiles of white matter properties: automating fiber-tract quantification. PLoS ONE 7, e49790.

Yeatman, J.D., Rauschecker, A.M., Wandell, B.A., 2013. Anatomy of the visual word form area: adjacent cortical circuits and long-range white matter connections. Brain Lang. 125, 146–155.

Yeatman, J.D., Wandell, B.A., Mezer, A.A., 2014a. Lifespan maturation and degeneration of human brain white matter. Nat. Commun. 5, 4932.

Yeatman, J.D., Weiner, K.S., Pestilli, F., Rokem, A., Mezer, A., Wandell, B.A., 2014b. The vertical occipital fasciculus: a century of controversy resolved by in vivo measurements. Proc. Natl. Acad. Sci. U. S. A. 111, E5214–E5223.

Yoshimine, S., Ogawa, S., Horiguchi, H., Terao, M., Miyazaki, A., Matsumoto, K., Tsuneoka, H., Nakano, T., Masuda, Y., Pestilli, F., 2018. Age-related macular degeneration affects the optic radiation white matter projecting to locations of retinal damage. Brain Struct. Funct. 223, 3889–3900.

You, Y., Joseph, C., Wang, C., Gupta, V., Liu, S., Yiannikas, C., Chua, B.E., Chitranshi, N., Shen, T., Dheer, Y., Invernizzi, A., Borotkanics, R., Barnett, M., Graham, S.L., Klistorner, A., 2019. Demyelination precedes axonal loss in the transneuronal spread of human neurodegenerative disease. Brain 142, 426–442.

Zhang, H., Schneider, T., Wheeler-Kingshott, C.A., Alexander, D.C., 2012. NODDI: practical in vivo neurite orientation dispersion and density imaging of the human brain. Neuroimage 61, 1000–1016.

Zhou, W., Muir, E.R., Chalfin, S., Nagi, K.S., Duong, T.Q., 2017. MRI Study of the Posterior Visual Pathways in Primary Open Angle Glaucoma. J. Glaucoma 26, 173–181.